HSPI The Open Access Publisher

JSMT JOURNAL OF SPORTS MEDICINE AND THERAPY
ISSN 2573-1726

Research Article

Anatomy and biomechanics of the rat knee ligaments

Zhe Song[1,2]*, Xiang-Hua Deng[1], Scott Rodeo[1], Zoe M Album[1], Arielle Hall[1], Tina Chen[1], Brett Croen[1] and Rodeo A Scott[1]*

[1]Orthopedic Soft Tissue Research Program, Hospital for Special Surgery, 535 E 70th, New York, NY 10021, USA

[2]Honghui Hospital, Xian Jiaotong University, Xian, China

Abstract

In this study, the authors systematically examined the anatomical and biomechanical properties of the ligaments in the normal rat knee. These biomechanical data will facilitate the use of the rat knee model for future studies of knee ligament injury, repair, and reconstruction. Fifty-six fresh cadaver male Sprague-Dawley rats, aged 16 weeks, were used for this study, with 48 rats for biomechanical testing and 8 for micro-CT and histological evaluation. Our findings suggest that the gross anatomy of the rat knee joint and ligaments is very similar to humans despite some minor differences and features unique to the rat knee. The patella tendon and ACL are the two strongest soft tissue structures in the rat knee joint, with the highest failure force and stiffness, and both play a role in the anterior stability of the knee. In comparison, the failure force and stiffness of the LCL is half of the MCL, suggesting that other structures, such as the popliteal tendon, may play some role in lateral knee stabilization besides the LCL. In addition, our data suggest that anterior knee stability was improved after ACL reconstruction, but was not fully restored to intact ACL function. In conclusion, our study indicates the anatomical and biomechanical properties of the knee joint and ligaments of rat knees. Then we could confirm a reproducible and realistic rat model of knee ligaments like the clinical cases, and provide a basis for the study of knee ligament biology that simulates techniques used in humans.

More Information

***Address for Correspondence:** Zhe Song, Orthopedic Soft Tissue Research Program, Hospital for Special Surgery, 535 E 70th, New York, NY 10021, USA, Honghui Hospital, Xian Jiaotong University, Xian, China, Email: sz0494@163.com

Rodeo A Scott, Orthopedic Soft Tissue Research Program, Hospital for Special Surgery, 535 E, 70th, New York, NY 10021, USA, Email: rodeos@hss.edu

Submitted: April 17, 2023
Approved: April 26, 2023
Published: April 27, 2023

How to cite this article: Song Z, Deng XH, Rodeo S, Album ZM, Hall A, et al. Anatomy and biomechanics of the rat knee ligaments. J Sports Med Ther. 2023; 8: 008-015.

DOI: 10.29328/journal.jsmt.1001065

Keywords: Rat knee; Ligaments; Biomechanics; CT image

Introduction

The knee joint has the anatomical characteristics and biomechanical roles to allow gait, flexion, and rotation while transmitting forces across it and remaining stable during the activities of daily life. The knee joint acts as a pivot between the two longest bones in the human body. And even though the strongest muscles in the body (the quadriceps muscles, which extend into the patellar tendon (PT)) act across it and some indispensable ligaments (anterior cruciate ligament (ACL), posterior cruciate ligament (PCL), lateral collateral ligament (LCL), medial collateral ligament (MCL)) act around it, knee ligament injuries are still common, particularly in sports and sports-related activities. Rupture of these ligaments (PT, ACL, PCL, LCL, and MCL) upsets the balance between knee mobility and stability, resulting in abnormal knee kinematics and damage to other tissues in and around the joint. This leads to morbidity and pain. A thorough knowledge of the complex anatomy and biomechanical function of the structures of the knee is essential in making accurate clinical diagnoses and decisions regarding the treatment of the multiple-ligament-injured knee [1].

Ninety percent of knee ligament injuries involve the ACL and MCL, which can lead to significant short- and long-term morbidity, such as chronic pain, joint instability, laxity, and possibly osteoarthritis [2-5]. Furthermore, with around 250,000 injuries per year in the United States, mainly affecting patients between 15 and 45 years of age, the ACL is the most commonly injured ligament [6,7]. Surgical reconstruction of the ACL is required to fully restore knee stability and possibly mitigate against progressive meniscus pathology and subsequent degeneration, thus surgery is the typical treatment for individuals who wish to return to an active lifestyle or for those with physically demanding occupational or sporting pursuits [8,9].

Because the ACL is extremely susceptible to injury and the ruptured ACL is unable to heal without surgical intervention, the limitations in activities of daily life as well as participation in sports drive over 250,000 patients to undergo surgery each year. ACL reconstructions result in an estimated direct cost of 3 billion dollars annually in the United States [10]. Currently, reconstruction of the anterior cruciate ligament (ACL) using a tendon graft is a commonly performed surgical procedure. The treatment strategies include ligament reconstruction using either autografts (such as semitendinosus and/or

gracilis) or allografts (such as semitendinosus, and tibialis tendon) [11]. While the majority of ligament reconstructions yield good clinical results, up to 20% - 25% of patients experience complications including recurrent instability that can progressively damage other knee structures [12]. Thus, there has been a tremendous quest for knowledge to better understand ligament injuries, healing, and remodeling with the hope to develop new and improved treatment strategies.

During the past three decades, significant advances have been made in characterizing the anatomical and biomechanical properties of the knee joint and ligaments as individual components as well as their contribution to joint function. Appropriate animal models are necessary to better understand the biological process and biomechanical role of graft-bone interface healing. Several different animal models have been used to study the basic biological and biomechanical aspects of ligament healing including goat, sheep, dog, pig, and rabbit models [13-17]. Compared to other large animals, the knee anatomy, geometry, structures, and basic biological processes of rat knees are very similar to those of the human knee. Rodent models are being used with increasing frequency to study the biological and biomechanical properties of knee ligament reconstruction procedures [18-22].

However, there are still some uncertainties about the anatomical characterization and biomechanical properties of the rat knee model that have precluded its use for the research of knee ligaments. Therefore, the study of anatomical characterization and biomechanical properties of the rat knee and ligaments is essential to verify the feasibility and reliability of a rat knee model for the experimental study of ligament injury, reconstruction, and healing process. It will also serve as a benchmark for further animal studies. To our knowledge, the anatomical and biomechanical properties and all intact knee ligaments in the rat knee are rarely reported. These baseline biomechanical data are critical for experimental studies of ligament injury, reconstruction, and healing processes in rats. The purpose of this study was to (1) define the anatomical features of the rat knee joint, (2) describe the biomechanical properties of the knee ligament (PT, ACL, PCL, MCL, LCL), and (3) evaluate the effect of joint stability after ACL injury.

Methods

This study was performed under the ethical approval of the Institutional Animal Care and Use Committee. Cadaveric rats were used for this study. A total of 56 fresh cadavers male Sprague-Dawley rats, aged 16 weeks (weight 260-300 Grams) were used for this study, with 48 rats for biomechanical testing and 8 for micro-CT and histological evaluation. All rats were 3 months of age and weighed between 300 and 350 g. Prior to these experiments, all right knee rats were used for the study of live ACL reconstruction. Each rat's hind leg was carefully dissected from surrounding tissues, keeping the major ligaments intact. The specimens were kept moist and wrapped in phosphate-buffered saline-soaked gauze.

Biomechanics of Knee ligaments

The entire lower extremity was harvested immediately after the animals were sacrificed and then frozen to 80 °C. At the time of biomechanical testing, the specimens were thawed to room temperature. Meticulous dissection under a loupe magnification was performed to remove all soft tissue around the knee, including the joint capsule and meniscus, while maintaining the ligament of interest. The PT, ACL, PCL, MCL, and LCL were dissected separately. The tibia and femur were each placed in a 2.0-mL cryogenic tube (VWR, Bridgeport, NJ) and embedded in liquid cement crack filler (Bondo Lightweight Filler 265, 3M, St. Paul, MN). The knee was maintained at a 35-degree flexion angle for biomechanical testing in order to measure the maximal tensile failure force of each ligament. The specimens were loaded in a custom-designed material testing system with a loading rate of 10 mm/min (0.167 mm/s) (Figure 1). The load-to-failure (N) and stiffness (N/mm) data were recorded and calculated from the linear portion of the load-displacement curve using Microsoft Excel (Microsoft Inc, Redmond, WA). The site of ligament failure (substance rupture, bone insertion, or growth plate fracture) was also recorded.

Kinematic of the normal knee joint and ACL deficiency knee

Eight rat knees were used for joint biomechanical tests. A custom-made knee tester was used for this study which can control the knee joint anterior-posterior motion. To mount the knee to the tester rigidly and control the knee motion, two 0.9 mm threaded pins were placed in the distal femur and two pins were placed in the proximal tibia. The knee was then mounted at 90 degrees of flexion on the custom testing device, which allowed the tibia to move anteriorly and posteriorly while constraining rotation. The sequence of testing was: 1. Intact ACL, 2. ACL transection. During the biomechanical testing, the tibia was moved anteriorly 1 mm and then the force and displacement data were collected (Figure 2).

Micro-CT analysis

The osseous morphology of rat knees was evaluated using high-resolution using nanofocus CT in a GE Phoenix Nanotom MTM instrument (GE Inspection Technologies; Lewiston, PA). For micro-CT analysis, the muscle and soft tissue from the leg were removed following sacrifice. The lower extremity was then placed in formalin overnight for fixation and soaked in

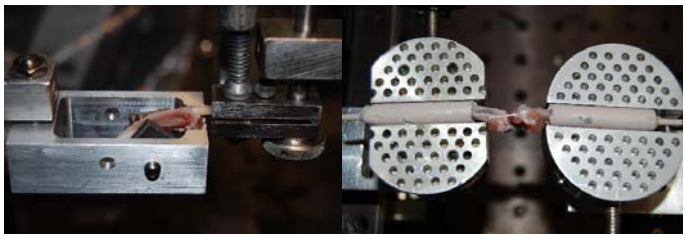

Figure 1: Biomechanical test of knee ligaments (Left, patella tendon test; right, knee ligament test).

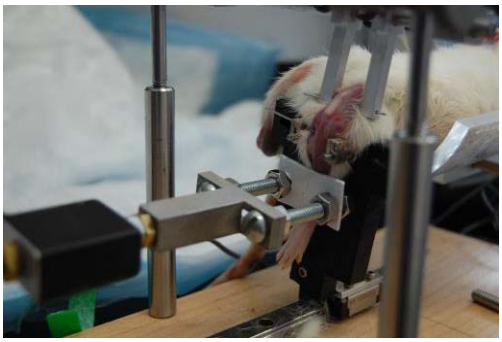

Figure 2: Biomechanical test of ACL intact, transection, and reconstruction.

PBS solution. Micro-CT analysis was performed in 8 animals using a Scanco mCT 35 (Scanco Medical, Brü ttisellen, Switzerland) system. Imaging was performed with 6 µm voxel size at 55 KVp, 0.36 degrees rotation step (180 degrees angular range), and a 400ms exposure per view. Scanco micro-CT software (HP DEC Windows Motif 1.6) was utilized for image viewing, image analysis, 3D reconstruction, and thresholding of images. After 3D reconstruction, volumes were segmented using a global threshold of 0.4 g hydroxyapatite (HA)/ml. Bone morphometrics was measured in regions of interest of the cortex and trabecular bone; these regions were 3 mm proximal to the growth plate (metaphysis) in the distal femur and 3 mm distal to the growth plate (metaphysis) in the tibia in the cross-sectional plane. These same measurements were calculated for the epiphyseal regions of the femur and tibia in the sagittal plane.

Histological analysis

Rat hindlimbs were removed and fixed in 10% formalin solution followed by decalcification for 3 days (Immunocal, Decal Chemical Corp, Tallman, NY). The tissues were then dehydrated, trimmed, and embedded in paraffin wax. Serial 5-µm-thick sections were cut in the sagittal and coronal plane using a microtome. Following sectioning, the 5-µm-thick sections were placed on slides and stained with hematoxylin-eosin (HE) and Safranin-O/Fast Green. The images were obtained using a Nikon Eclipse Ni-E microscope, using transmitted light at 4, 10, and 20X magnifications.

Statistical analysis

Qualitative descriptions are presented to describe the gross anatomy of the knee joint. Descriptive statistics were used to present means and standard deviations for the measurements of ligament dimensions, load to failure, and stiffness. Graph Pad Prism 7 software was utilized for joint biomechanics analysis, and the Mann-Whitney U test was used to compare groups. Statistical significance was set to $p < 0.05$.

Results

General

A total of 40 rat knees were used for the knee ligament and tendon testing, including 9 for PT, 10 for ACL, 7 for PCL, 7 for MCL, and 7 for LCL. The failure force (N), stiffness (N/mm) data, and the failure site are reported in Table 1. A total of 8 male Sprague-Dawley rats were used for knee joint biomechanics. The load-to-displacement data of ACL intact, transection, and reconstruction were recorded in sequence (Figure 1). Rat knees (n = 8) were first used for micro-CT analysis, and then were available for histological analysis (4 for sagittal plane and 4 for coronal plane).

Gross anatomical analysis

The gross inspection of the rat knee joint and ligaments demonstrated distinct similarities to human knee anatomy. As the continuation of the femoral quadriceps tendon, the PT extends from the inferior pole of the patella and inserts on the tibial tubercle. The ACL inserts in the intercondylar notch at the posteromedial edge of the lateral femoral condyle and projects to the anterior aspect of the tibial intercondylar eminence, adjacent to the anterior insertion of the medial meniscus. The PCL inserts in the intercondylar region at the anterolateral edge of the medial femoral condyle and projects posteriorly and inferiorly to the tibial intercondylar area. The MCL courses from the medial femoral epicondyle to the tibia, while the LCL courses obliquely and posteriorly from the lateral femoral epicondyle to the fibular head. However, one difference is that the extensor digitorum longus tendon (EDLT) crosses the joint and attaches to the lateral femoral condyle, running parallel and anterior to the LCL (Figure 3).

Biomechanical analysis

Knee ligaments biomechanics: The biomechanical

Figure 3: Gross anatomy of the rat knee joint and ligaments. (A: LCL\Flexor Digital Tendon\Popliteus Tendon; B: ACL; C: PCL; D: MCL; E: LCL; F: ACL; G: PCL; H: MCL; I: ACL; K: PCL).

Table 1: Biomechanical test and statistical data: failure force, stiffness, and failure site of rat knee ligaments.

Ligament	Failure Force(N)	Stiffness(N/mm)	Failure Site	Comparison of failure force (*p* - value)	Comparison of stiffness (*p* - value)
PT (*n* = 9)	70.34 ± 7.49	35.87 ± 6.85	Substance(7/9)	PT *vs.* ACL(<0.0001[a])	PT *vs.* ACL(0.2562)
			Tibial fracture(*n* = 2)	PT *vs.* PCL(<0.0001[a])	PT *vs.* PCL(<0.0001[a])
				PT *vs.* MCL(<0.0001[a])	PT *vs.* MCL(<0.0001[a])
				PT *vs.* LCL(<0.0001[a])	PT *vs.* LCL(<0.0001[a])
ACL	51.09 ± 4.41	32.77 ± 3.97	Substance(6/10)	ACL *vs.* PCL(<0.0001[a])	ACL *vs.* PCL(0.0002[a])
			Tibial growth plate fracture(4/10)	ACL *vs.* MCL(<0.0001[a])	ACL *vs.* MCL(<0.0001[a])
				ACL *vs.* LCL(<0.0001[a])	ACL *vs.* LCL(<0.0001[a])
PCL	23.81 ± 3.35	19.48 ± 5.07	Substance(1/7)	PCL *vs.* MCL(0.9933)	PCL *vs.* MCL(0.0122[a])
			Tibial growth plate fracture(2/7)	PCL *vs.* LCL(<0.0001[a])	PCL *vs.* LCL(0.0006[a])
			Femoral insertion(4/7)		
MCL	23.79 ± 5.16	12.73 ± 2.66	Femoral growth plate fracture(1/7)	MCL *vs.* LCL(0.0010[a])	MCL *vs.* LCL(0.0012[a])
			Tibial insertion(6/7)		
LCL	12.78 ± 1.47	7.33 ± 1.01	Fibular head fracture (6/7)		
			Fibular avulsion (1/7)		

Abbreviations: PT: Patellar Tendon; ACL: Anterior Cruciate Ligament; LCL: Lateral Collateral Ligament; MCL: Medial Collateral Ligament; PCL: Posterior Cruciate Ligament. Value note: Mean standard deviation; *p* - values calculated by Mann-Whitney U test. The *p* - values < 0.05 (in bold) are considered to represent statistical significance.

testing showed that the PT had the highest failure force (70.34 ± 7.49 N), followed by the ACL (51.09 ± 4.41N). The PCL (23.81 ± 3.35N) and the MCL (23.79 ± 5.16 N) were similar and approximately half the strength of the ACL. Finally, the LCL had the lowest load to failure (12.78 ± 1.47N). The failure force of the PT was significantly higher than all knee ligaments ($p < 0.05$), and the ACL was significantly higher than the PCL ($p < 0.05$), MCL ($p < 0.05$), and LCL ($p < 0.05$). There was no significant difference between the PCL and MCL ($p > 0.05$) and the LCL had a significantly lower failure load than all other knee ligaments ($p < 0.05$). (Table 1).

The stiffness of the PT (35.87 ± 6.85 N/mm) and ACL (32.77 ± 3.97 N/mm) were similar, and higher than the PCL (19.48 ± 5.07N/mm) and MCL (12.73 ± 2.66/mm). Additionally, the LCL had the lowest stiffness (7.33 ± 1.01N/mm). There was no significant difference between the stiffness of the PT and ACL ($p > 0.05$). However, both the PT and ACL were significantly higher than the PCL ($p < 0.05$), MCL ($p < 0.05$), and LCL ($p < 0.05$). There was no significant difference in stiffness between the PCL and MCL ($p > 0.05$), while the LCL had significantly lower stiffness than all other knee ligaments ($p < 0.05$) (Table 1).

Seven of the PT specimens (7 of 9, 78%) and six of the ACL specimens (6 of 10, 60%) failed in the mid-substance, while most of the PCL specimens failed at the femoral insertion site (4 of 7, 57%). In addition, six of the MCL specimens failed at the tibial insertion (6 of 7, 86%) and six of the LCL specimens failed by fibular head fracture (6 of 7, 86%) (Table 1).

Joint biomechanics

The intact ACL had the highest force required to translate the tibia anteriorly by 1 mm (37.69 ± 9N), while after ACL transection the translation force was 9. ± 3.991N ($p = 0.00004$) (Figure 4).

Micro-CT analysis of rat knee osseous morphology

The osseous morphology of the rat knee (tibia, femur, and patella) was detailed successfully at high resolution (5 µm voxel resolution) using micro-CT. The micro-CT images showed that the rat tibia plateau is convex, in contrast to the human tibia plateau which is inclined approximately 7 degrees posterior. The curvature of the femoral condyles increased markedly posteriorly, where there is a medial and lateral fabella. The concave patella articulates with the femoral sulcus or anterior articular surface of the distal femur, which is a coalescence of the medial and lateral femoral condyles. The intercondylar area of the rat tibia forms a distinct depression and there are well-developed medial and lateral menisci, which articulate with the femoral and tibial condyles and are rotated orthogonal to the long axis of the bones. The growth plate on both the femoral and tibial sides separates the epiphyseal and metaphyseal areas (Figure 5).

Trabecular bone parameters were also measured on micro CT in both the metaphysis and epiphysis of the rat femur and tibia. The data on bone fraction, trabecular number, and their morphology and spatial relationship (TbTh, separation, and connectivity) in the metaphyseal and epiphyseal regions are summarized in Table 2. Cortical bone measurements were focused on the epiphyseal regions using distance transform methods (Table 3).

Focused analysis of the epiphyseal regions permitted observation of subchondral bone characteristics for the femoral condyles (bone volume fraction: 0.65 _ 0.02%; TMD: 914.69 _ 20.20 mg HA/mL) and tibial plateau (bone volume fraction: 0.78 _ 0.12%; TMD: 885.96 _ 17.40 mg HA/cm^3).

Histological analysis

The histological evaluation demonstrated a typical ligament appearance with well-aligned, parallel collagen bundles. Cells were generally aligned parallel to the collagen fibers. HE and Safranin O/fast green staining demonstrated fibrocartilaginous transition zones at the attachments of the ACL and PCL, consistent with a direct type of insertion (Figure 6). The LCL also had a direct insertion morphology

Table 2: Micro CT morphometrics: analysis of trabecular bone.

Variable	Abbreviation of Variable	Femur (metaphysis)	Femur (epiphysis)	Tibia (metaphysis)	Tibia (epiphysis)	Units	Description
Bone volume fraction	BV/TV	20.95 ± 1.25	36.20 ± 4.97	20.72 ± 2.69	41.21 ± 1.07	%	Ratio: segmented bone to the total volume of the region of interest
Trabecular number	Tb.N	6.46 ± 0.38	7.67 ± 1.13	6.57 ± 0.64	9.11 ± 1.35	1/mm	The average number of trabecular units per unit
Trabecular thickness	TbTh	0.06 ± 0.011	0.05 ± 0.005	0.05 ± 0.003	0.06 ± 0.004	mm	Mean thickness of the trabecular units
Trabecular separation	Tb.Sp	0.15 ± 0.009	0.13 ± 0.016	0.15 ± 0.013	0.12 ± 0.019	mm	Mean distance between trabeculae
Tissue mineral density	TMD	754.94 ± 43.19	805.60 ± 54.10	712.84 ± 27.67	799.43 ± 37.14	mg HA/ml	Tissue mineral density of bone tissue only
Connectivity density	Conn.D	217.52 ± 9.9	374.02 ± 49.45	243.35 ± 28.74	390.17 ± 48.51	mm^3	Degree of connectivity of the trabeculae

Abbreviation: CT: Computed Tomography; HA: Hydroxyapatite; Value note: Mean ± standard deviation.

Table 3: Micro CT morphometrics: analysis of cortical bone.

Variable	Abbreviation of Variable	Femur (metaphysis)	Tibia (metaphysis)	Units	Description
Total cross-sectional area	Tt.Ar	1.49 ± 0.85	2.90 ± 0.42	mm^2	The total cross-sectional area inside the periosteal envelope
Cortical bone area	Ct.Ar	0.64 ± 0.34	1.38 ± 0.15	mm^2	Cortical volume divided by the number of slices _ thickness
Cortical area fraction	Ct.Ar/Tt.Ar	0.45 ± 0.06	0.48 ± 0.03	%	The ratio of cortical bone area and cross-section
Average cortical thickness	Ct.Th	0.08 ± 0.03	0.54 ± 0.28	mm	Cortical thickness
Moment of inertia (max)	Imax	0.34 ± 0.16	0.87 ± 0.15	mm^4	Maximum moment of inertia
Moment of inertia (min)	Imin	0.20 ± 0.12	0.61 ± 0.10	mm^4	Minimum moment of inertia
Polar moment of inertia	J	0.54 ± 0.28	1.47 ± 0.25	mm^4	Polar moment of inertia

Abbreviation: CT: Computed Tomography; Value note: Mean ± standard deviation.

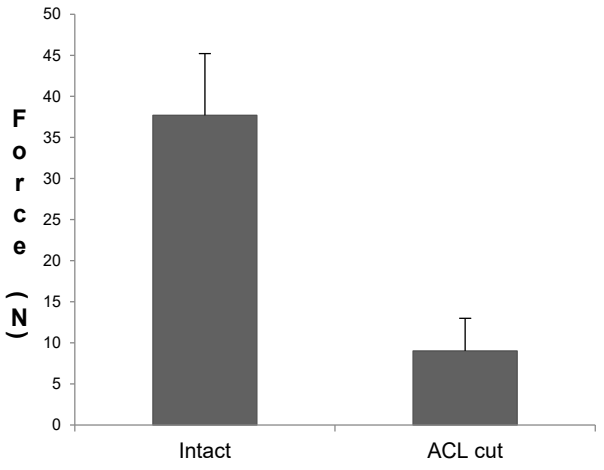

Figure 4: The force required to translate the tibia anteriorly by 1 mm.

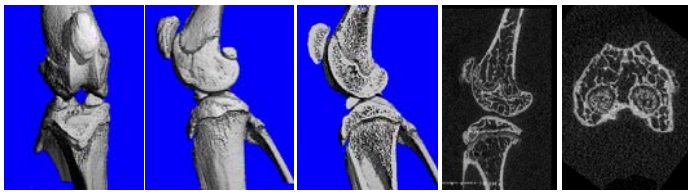

Figure 5: Osseous Morphology of the rat knee joint and cross-sectional anatomy with osseous detailing.

on both the femoral and fibular attachments. In contrast, the MCL insertion was a direct type of insertion on the femoral side and an indirect type on the tibial side, with collagen fibers blending with the underlying joint capsule, periosteum, and bone and an absence of a zone of intervening fibrocartilage (Figure 7).

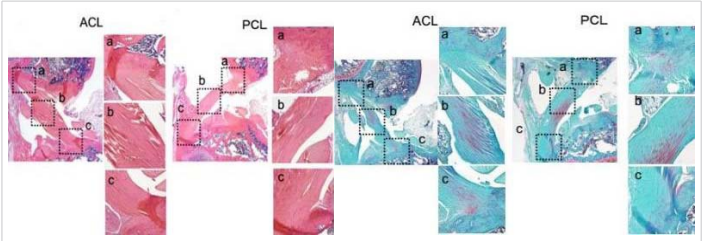

Figure 6: Sagittal plane section showing ACL and PCL at 4 magnification and their direct insertions, respectively (HE and safranin-O staining) at 20 magnification (a-c).

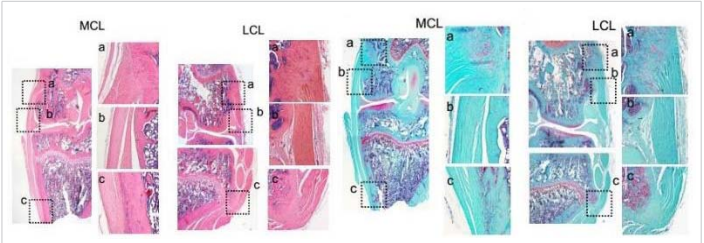

Figure 7: Coronal plane section showing ACL and PCL (HE and safranin-O staining) at 4 magnification. The LCL direct insertions and MCL direct and indirect insertion (HE and safranin-O staining) at 20 magnification (a-c).

Discussion

Previous studies have examined different animal models (goat, sheep, dog, pig, and rabbit) to better understand the mechanism of knee ligament injuries, healing, and remodeling [13-17]. However, rodent models are being used with increasing frequency to study the biological and biomechanical properties of ligament healing due to cost considerations, the availability of immunohistochemical and molecular reagents, and the ability to better control the post-surgical mechanical loading environment [18-22].

In this descriptive study, we have characterized the anatomical and biomechanical properties of the osseous and ligamentous structures of the rat knee. Overall, our evaluation of the rat knee joint and ligaments suggests that the basic anatomical and biomechanical characteristics of the rat knee are similar to the human knee. The purpose of this work is to provide baseline information to allow the use of the rat knee as a feasible and reproducible translational platform for further study of the biology and biomechanics of knee ligament reconstruction/repair and healing.

The gross anatomy of the osseous and ligamentous structures of the rat knee is highly analogous to the human knee, suggesting a similar function. Furthermore, the femoral and tibial/fibular attachments of all the knee ligaments are also similar to the human knee. The PT originates from the quadriceps tendon attached to the top of the patella, extends from the inferior pole of the patella, and inserts on the tibial tubercle [23-25]. Both the ACL and PCL are situated within the knee joint, originate from the femoral condyle, and insert into the tibial intercondylar area. They stabilize the knee by limiting the rotation and the anterior/posterior translation of the tibia. While the MCL and LCL are similar to human MCL and LCL in that they are attached outside of the knee joint, they have origins close to the epicondyle axis on each side of the femur and insert into the proximal tibia and fibula, respectively. The failure force of LCL is only half of MCL and is similar to the human. Similarly, the failure force and stiffness of the rat LCL is half of the MCL, suggesting that other structures, such as the popliteal tendon and/or capsule, contribute to lateral knee stabilization as in humans. These ligaments provide valgus/varus stability to the joint. Our joint biomechanical data showed that minimal force (9N) is required to translate the tibia 1 mm anteriorly after ACL transection. This translation force is only a quarter of the intact ACL force (37.9 N), demonstrating that the ACL plays a very important role in anterior knee stability.

However, there are some notable differences in the gross anatomy between the rat knee and the human knee. The rat knee has an additional intra-articular attachment of the extensor digitorum longus tendon to the lateral femoral epicondyle. This anatomical characteristic is shared with other quadrupedal animals including the cow, sheep, goat, dog, pig, rabbit, and mouse [26-29] and likely plays an important role in knee anterior stability and dorsiflexion of the forefoot, especially during knee flexion. The osseous morphology of the tibia plateau of rat knees is lower on the sides with a ridge in the center, while the tibia plateau of the human knee has a posterior slope. This is not particularly surprising since the rat is quadrupedal and ambulates with its knees in higher degrees of flexion throughout the weight-bearing and gait cycle. Another difference is the presence of a distinct depression in the intercondylar area of the rat tibia and the persistence of the growth plate in the long bones of the sexually mature rat. At 3 months of age, although the rat skeleton is considered relatively mature their growth plates are still open at this point and will close much later than humans. Moreover, the presence of bilateral fabella is a prominent feature in rats and is less common in humans. These medial and lateral sesamoid bones are consistently located in each head of the gastrocnemius muscle [30-33].

Micro CT analysis represents the gold standard in quantifying the microstructure of bone in small animal models.

We measured bone morphometrics in regions of interest of the cortex and trabecular bone that would be surgically exposed by transarticular bone tunnel for graft fixation. These regions were 3 mm proximal to the growth plate (metaphysis) in the distal femur and 3 mm distal to the growth plate (metaphysis) in the proximal tibia. In addition, these regions of metaphyseal and epiphyseal bone may be most susceptible to altered biomechanical loading following knee ligamentous injury (Tables 2,3). Bone volume fraction, TbN, TMD, and trabecular Conn-D were higher in the epiphyseal region compared with the metaphyseal region in both the femur and tibia, likely due to mechanical loading of the joint surface with ambulation. The analysis of cortical bone showed that all parameters of bone morphology, connectivity, and spatial distribution of trabecular architecture were higher in the tibial metaphysis than the femoral metaphysis, which may have implications for graft fixation and healing using a rat model of ACL reconstruction.

At the microscopic level, the histological properties such as overall matrix appearance, collagen fiber structure, vascularity, cellularity, and enthesis of the rat knee ligaments are also similar to the human knee ligaments. The collagen, matrix, and cells that make up the ligaments are grouped into bundles with a characteristic organization and crimp that allows the ligament to respond to mechanical loading due to joint motion. Ligaments of rat knee attach to the bone by the interdigitation of the collagen fibers, with a fibrocartilaginous transition zone (direct insertion) at the ACL, PCL, LCL, and MCL (on the femoral side) insertion site, while the MCL inserts to the bone via Sharpey's fibers (indirect insertion) on the tibial side [34,35].

Our biomechanical data for knee ligaments suggests that the rat PT and ACL are the two strongest soft tissue structures in the rat knee joint, with the highest failure force and stiffness, and play a role in the extension of the knee and prevention of anterior instability of the knee. The strength of the PCL is similar to the MCL, while the LCL has a minimal failure force and stiffness at approximately half the strength of the PCL and the MCL. This indicates that other structures, such as the popliteal tendon, may play some role in lateral knee stabilization besides the LCL. This biomechanical data is similar to the pattern seen in the human knee [36,37]. The majority of PTs and ACLs of the rat knee failed at the site of ligament substance during our biomechanical testing, which

is analogical to the human knee [38]. On the other hand, most of the PCLs and MCLs failed by femoral and tibial insertion, respectively. The failure sites of LCL are mainly all fibular head fractures. The reasons for the different failure sites in different ligaments still remain unclear. However, it is probably due to the persistence of the physes, and the biomechanical properties of the rat knee ligaments in the model.

Our joint biomechanical analysis showed that the rat knee with intact ACL had the highest force to resist the tibia anteriorly by 1 mm, followed by the reconstructed ACL model, and then the transected ACL model with the lowest force. We found that the anterior knee stability of the transected ACL rat certainly improved after ACL reconstruction, but was not fully restored to the intact ACL function. These findings demonstrate the difficulty in restoring knee stability following ACL reconstruction in the rat knee. Comparing the force required to translate the tibia anteriorly by 1 mm, the intact ACL group was significantly higher than the ACL reconstruction group and ACL transection group. However, the ACL reconstruction group was slightly higher than the ACL transection group but the difference was not significant. This is consistent with prior studies demonstrating the difficulty in restoring anterior stability in other animal models of ACL reconstruction.

The major limitations of this article include the small size of the rat knee and ligaments, the absence of immune-histochemical data to identify specific matrix proteins and cell phenotype in rat ligaments, and the unknown translation of quadruped models to humans. In addition, the procedure requires the development of microsurgical skills and has a substantial learning curve.

In conclusion, our study indicates that the macro- and microstructural and biomechanical properties of the knee joint and ligaments of the rat knee provide a reproducible and realistic model that provides a basis for further study of knee ligament biology using surgical reconstruction techniques similar to those used in humans. Despite the small dimensions, our biomechanical analysis suggests the potential for the use of a rat model to enhance our understanding of the biological processes involved in knee ligament injury, repair, and reconstruction on a cellular and molecular level. This initial report provides important baseline data to support further use of rat models to study knee ligament biology and pathology, helping to ultimately identify methods to improve healing in our patients [39,40].

Author contributions statement

Scott A. Rodeo and Xiang-Hua Deng designed experiments; Scott Rodeo Jr., Zoe M. Album, Arielle Hall, and Tina Chen carried out experiments; Zhe Song analyzed experimental results and wrote the manuscript. Brett Croen assisted with the amendment of the manuscript.

References

1. Bonasia D, Ross P, Rossi R. Anatomy and Biomechanics of the Knee. Orthopedic Sports Medicine. Springer Milan.
2. Miyasaka K, Daniel D, Stone M. The incidence of knee ligament injuries in the general population. American Journal of Knee Surgery. 1991.
3. Griffin LY, Albohm MJ, Arendt EA, Bahr R, Beynnon BD, Demaio M, Dick RW, Engebretsen L, Garrett WE Jr, Hannafin JA, Hewett TE, Huston LJ, Ireland ML, Johnson RJ, Lephart S, Mandelbaum BR, Mann BJ, Marks PH, Marshall SW, Myklebust G, Noyes FR, Powers C, Shields C Jr, Shultz SJ, Silvers H, Slauterbeck J, Taylor DC, Teitz CC, Wojtys EM, Yu B. Understanding and preventing noncontact anterior cruciate ligament injuries: a review of the Hunt Valley II meeting, January 2005. Am J Sports Med. 2006 Sep;34(9):1512-32. doi: 10.1177/0363546506286866. PMID: 16905673.
4. Carlson K. Assessment of post-rehabilitation ACL reconstructed knees. Australian International Academic Centre. 2020.
5. Lohmander LS, Ostenberg A, Englund M, Roos H. High prevalence of knee osteoarthritis, pain, and functional limitations in female soccer players twelve years after anterior cruciate ligament injury. Arthritis Rheum. 2004 Oct;50(10):3145-52. doi: 10.1002/art.20589. PMID: 15476248.
6. Strauss EJ, Barker JU, Bach BR. Osteoarthritis in the anterior cruciate ligament-deficient knee epidemiology, biomechanics, and effects on the meniscus and articular cartilage. 2010.
7. Leumann A, Leonard T, Nüesch C, Horisberger M, Mündermann A, Herzog W. The natural initiation and progression of osteoarthritis in the anterior cruciate ligament deficient feline knee. Osteoarthritis Cartilage. 2019 Apr;27(4):687-693. doi: 10.1016/j.joca.2019.01.003. Epub 2019 Jan 11. PMID: 30641135.
8. Kim YM, Lee CA, Matava MJ. Clinical results of arthroscopic single-bundle transtibial posterior cruciate ligament reconstruction: a systematic review. American Journal of Sports Medicine. 2011; 27(2): 141.
9. Race A, Amis AA. The mechanical properties of the two bundles of the human posterior cruciate ligament. J Biomech. 1994 Jan;27(1):13-24. doi: 10.1016/0021-9290(94)90028-0. PMID: 8106532.
10. Frobell RB, Roos EM, Roos HP, Ranstam J, Lohmander LS. A randomized trial of treatment for acute anterior cruciate ligament tears. N Engl J Med. 2010 Jul 22;363(4):331-42. doi: 10.1056/NEJMoa0907797. Erratum in: N Engl J Med. 2010 Aug 26;363(9):893. PMID: 20660401.
11. Klimkiewicz JJ, Petrie RS, Harner CD. Surgical treatment of combined injury to anterior cruciate ligament, posterior cruciate ligament, and medial structures. Clin Sports Med. 2000 Jul;19(3):479-92, vii. doi: 10.1016/s0278-5919(05)70219-2. PMID: 10918961.
12. Woo SL, Chan SS, Yamaji T. Biomechanics of knee ligament healing, repair and reconstruction. J Biomech. 1997 May;30(5):431-9. doi: 10.1016/s0021-9290(96)00168-6. PMID: 9109554.
13. Meller R, Haasper C, Westhoff J, Brand J, Knobloch K, Hankemeier S, Hesse E, Krettek C, Jagodzinski M. An animal model to study ACL reconstruction during growth. Technol Health Care. 2009;17(5-6):403-10. doi: 10.3233/THC-2009-0561. PMID: 20051620.
14. Nguyen DT, Dellbrügge S, Tak PP, Woo SL, Blankevoort L, van Dijk NC. Histological characteristics of ligament healing after bio-enhanced repair of the transected goat ACL. J Exp Orthop. 2015 Dec;2(1):4. doi: 10.1186/s40634-015-0021-5. Epub 2015 Feb 28. PMID: 26914872; PMCID: PMC4544611.
15. Ma CB, Kawamura S, Deng XH, Ying L, Schneidkraut J, Hays P, Rodeo SA. Bone morphogenetic proteins-signaling plays a role in tendon-to-bone healing: a study of rhBMP-2 and noggin. Am J Sports Med. 2007 Apr;35(4):597-604. doi: 10.1177/0363546506296312. Epub 2007 Jan 11. PMID: 17218656.

16. Cai C, Chen C, Chen G, Wang F, Guo L, Yin L, Feng D, Yang L. Type I collagen and polyvinyl alcohol blend fiber scaffold for anterior cruciate ligament reconstruction. Biomed Mater. 2013 Jun;8(3):035001. doi: 10.1088/1748-6041/8/3/035001. Epub 2013 Mar 26. PMID: 23531980.

17. Rodeo SA, Kawamura S, Kim HJ, Dynybil C, Ying L. Tendon healing in a bone tunnel differs at the tunnel entrance versus the tunnel exit: an effect of graft-tunnel motion? Am J Sports Med. 2006 Nov;34(11):1790-800. doi: 10.1177/0363546506290059. Epub 2006 Jul 21. PMID: 16861579.

18. Zong JC, Ma R, Wang H, Cong GT, Lebaschi A, Deng XH, Rodeo SA. The Effect of Graft Pretensioning on Bone Tunnel Diameter and Bone Formation After Anterior Cruciate Ligament Reconstruction in a Rat Model: Evaluation With Micro-Computed Tomography. Am J Sports Med. 2017 May;45(6):1349-1358. doi: 10.1177/0363546516686967. Epub 2017 Feb 1. PMID: 28298055.

19. Carbone A, Carballo C, Ma R, Wang H, Deng X, Dahia C, Rodeo S. Indian hedgehog signaling and the role of graft tension in tendon-to-bone healing: Evaluation in a rat ACL reconstruction model. J Orthop Res. 2016 Apr;34(4):641-9. doi: 10.1002/jor.23066. Epub 2015 Nov 25. PMID: 26447744; PMCID: PMC6345400.

20. Rodeo SA, Voigt C, Ma R, Solic J, Stasiak M, Ju X, El-Amin S, Deng XH. Use of a new model allowing controlled uniaxial loading to evaluate tendon healing in a bone tunnel. J Orthop Res. 2016 May;34(5):852-9. doi: 10.1002/jor.23087. Epub 2015 Nov 25. PMID: 26509464.

21. Camp CL, Lebaschi A, Cong GT, Album Z, Carballo C, Deng XH, Rodeo SA. Timing of Postoperative Mechanical Loading Affects Healing Following Anterior Cruciate Ligament Reconstruction: Analysis in a Murine Model. J Bone Joint Surg Am. 2017 Aug 16;99(16):1382-1391. doi: 10.2106/JBJS.17.00133. PMID: 28816898.

22. Deng XH, Lebaschi A, Camp CL, Carballo CB, Coleman NW, Zong J, Grawe BM, Rodeo SA. Expression of Signaling Molecules Involved in Embryonic Development of the Insertion Site Is Inadequate for Reformation of the Native Enthesis: Evaluation in a Novel Murine ACL Reconstruction Model. J Bone Joint Surg Am. 2018 Aug 1;100(15):e102. doi: 10.2106/JBJS.16.01066. PMID: 30063598; PMCID: PMC6661256.

23. Flandry F, Hommel G. Normal anatomy and biomechanics of the knee. Sports Med Arthrosc Rev. 2011 Jun;19(2):82-92. doi: 10.1097/JSA.0b013e318210c0aa. PMID: 21540705.

24. Bowman KF, Sekiya JK. Anatomy and biomechanics of the posterior cruciate ligament and other ligaments of the knee. Operative Techniques in Sports Medicine. 2009; 17(3): 126-134.

25. Chhabra A, Elliott CC, Miller MD. Normal anatomy and biomechanics of the knee. Sports Medicine & Arthroscopy Review. 2001; 9(3): 166-177.

26. Proffen BL, McElfresh M, Fleming BC, Murray MM. A comparative anatomical study of the human knee and six animal species. Knee. 2012 Aug;19(4):493-9. doi: 10.1016/j.knee.2011.07.005. Epub 2011 Aug 17. PMID: 21852139; PMCID: PMC3236814.

27. Hildebrand C, Oqvist G, Brax L, Tuisku F. Anatomy of the rat knee joint and fibre composition of a major articular nerve. Anat Rec. 1991 Apr;229(4):545-55. doi: 10.1002/ar.1092290415. PMID: 2048758.

28. Carballo CB, Hutchinson ID, Album ZM, Mosca MJ, Hall A, Rodeo S Jr, Ying L, Deng XH, Rodeo SA. Biomechanics and Microstructural Analysis of the Mouse Knee and Ligaments. J Knee Surg. 2018 Jul;31(6):520-527. doi: 10.1055/s-0037-1604151. Epub 2017 Jul 18. PMID: 28719939.

29. Osterhoff G, Löffler S, Steinke H, Feja C, Josten C, Hepp P. Comparative anatomical measurements of osseous structures in the ovine and human knee. Knee. 2011 Mar;18(2):98-103. doi: 10.1016/j.knee.2010.02.001. Epub 2010 Feb 25. PMID: 20188573.

30. Duncan W, Dahm DL. Clinical anatomy of the fabella. Clin Anat. 2003 Sep;16(5):448-9. doi: 10.1002/ca.10137. PMID: 12903068.

31. Tobechukwu OK, Adeniyi OS, Olajide HJ, Tavershima D, Sulaiman SO. Macro–anatomical and morphometric studies of the Grasscutter (thryonomysswinderianus). Forelimb skeleton.

32. Jin ZW, Shibata S, Abe H, Jin Y, Li XW, Murakami G. A new insight into the fabella at knee: the foetal development and evolution. Folia Morphol (Warsz). 2017;76(1):87-93. doi: 10.5603/FM.a2016.0048. Epub 2016 Sep 26. PMID: 27665955.

33. Andriacchi TP, Favre J, Erhart-Hledik JC, Chu CR. A systems view of risk factors for knee osteoarthritis reveals insights into the pathogenesis of the disease. Ann Biomed Eng. 2015 Feb;43(2):376-87. doi: 10.1007/s10439-014-1117-2. Epub 2014 Sep 16. PMID: 25224078; PMCID: PMC4340713.

34. Woo S, Maynard J, Butler D, Lyon R, Oakes B. Ligament, tendon, and joint capsule insertions to bone. Injury & Repair of the Musculo Skeletal Soft Tissues. 1988.

35. Helito CP, Miyahara HS, Bonadio MB, Tirico LEP, Gobbi RG, Demange MK, Angelini FJ, Pecora JR, Camanho GL. Anatomical study on the anterolateral ligament of the knee. Rev Bras Ortop. 2013 Sep 27;48(4):368-373. doi: 10.1016/j.rboe.2013.04.007. PMID: 31304135; PMCID: PMC6565922.

36. Nielsen S, Kromann-Andersen C, Rasmussen O, Andersen K. Instability of cadaver knees after transection of capsule and ligaments. Acta Orthop Scand. 1984 Feb;55(1):30-4. doi: 10.3109/17453678408992307. PMID: 6702425.

37. Wilson WT, Deakin AH, Payne AP, Picard F, Wearing SC. Comparative analysis of the structural properties of the collateral ligaments of the human knee. J Orthop Sports Phys Ther. 2012 Apr;42(4):345-51. doi: 10.2519/jospt.2012.3919. Epub 2011 Oct 25. PMID: 22030378.

38. List J, Mintz DN, Difelice GS. The locations of anterior cruciate ligament tears in pediatric and adolescent patients: a magnetic resonance study. Journal of Pediatric Orthopaedics. 2017; 1.

39. Irvine JN, Arner JW, Thorhauer E, Abebe ES, D'Auria J, Schreiber VM, Harner CD, Tashman S. Is There a Difference in Graft Motion for Bone-Tendon-Bone and Hamstring Autograft ACL Reconstruction at 6 Weeks and 1 Year? Am J Sports Med. 2016 Oct;44(10):2599-2607. doi: 10.1177/0363546516651436. Epub 2016 Jul 13. PMID: 27411358.

40. Liu CF, Breidenbach A, Aschbacher-Smith L, Butler D, Wylie C. A role for hedgehog signaling in the differentiation of the insertion site of the patellar tendon in the mouse. PLoS One. 2013 Jun 10;8(6):e65411. doi: 10.1371/journal.pone.0065411. PMID: 23762363; PMCID: PMC3677907.